AP-1 regulates heterogeneous cellular dormancy in TNBC

Yang Dong[1] , Jin Bai[2] , Rong Fu[3], Huilan Su[1] , Shan Wu[1] , Dean G. Tang[1, 4,*], Jianjun Zhou[1,*]

[1]Research Center for Translational Medicine, Cancer Stem Cell Institute, Shanghai East Hospital, Tongji University School of Medicine, Shanghai, 200120, People's Republic of China

[2]Department of Oncology, Shanghai East Hospital, Tongji University School of Medicine, Shanghai, 200120, People's Republic of China.

[3]Core Facility of Basic Medical Sciences, Basic Medicine Faculty of Shanghai Jiao Tong University School of Medicine, Shanhai 200025, People's Republic of China

[4]Department of Pharmacology and Therapeutics, Roswell Park Comprehensive Cancer Center, Elm and Carlton Streets, Buffalo, NY 14263, USA

Key word: triple negative breast cancer, cancer dormancy, activating protein-1, cellular heterogeneity

Running title: AP-1 regulates heterogeneous cellular dormancy in TNBC

***Correspondence**: y_dong1239@163.com or Dean.Tang@Roswellpark.org or zhoujj_2000@aliyun.com.

Abstract

Dormant or slow cycling cells (SSCs) pre-exist in tumor and responsible for chemo-resistant and tumor recurrence. Label retaining is a common method to obtain live SCCs from tumor. Different label retaining methods have been developed, but there still haven't been reported whether different label retaining methods would result in same or different population of SCCs. We have utilized three label retaining methods simultaneously and identified overlapping but non-identical subpopulations of SCCs. These SCCs have similar yet different phenotypes in cell cycle, detoxification, motility and most importantly chemo-resistance. Gene profile shows three subpopulations of SCCs share similar gene expression pattern, and AP-1 subunit JunB overexpression is a key regulator of cellular dormancy. Inhibition of AP-1 could reduce drug resistance and tumor recurrence caused by SCCs, makes it a potential drug target for SCC elimination that could Improve patients' survival.

Introduction

Breast cancer is the most common malignant tumor in women, with the highest morbidity and mortality[1]. Among which, triple-negative breast cancer lacks effective targeted therapy due to the lack of specific markers. It has the worst prognosis among all breast cancer patients and is the most prone to recurrence and metastasis[2]. Currently, the commonly used clinical treatments are whether targeted drugs or anti-mitosis drugs. Previous studies have found that whether in the autopsy samples of tumor patients or cell lines cultured in vitro, there always pre-existed a group of dormant cells, or slow cycling cells (SSCs)[3]. However, due to the slow-cycling and relative low differentiation characteristics, slow cycling cells can survive from most clinical treatment, resulting in the formation of minimal residues or micro-metastasis. Some slow cycling cells can relapse after 5 years or even 10 years of dormancy[4]. Therefore, finding a slow cycling cells targeted therapy has positive clinical significance for the treatment of triple-negative breast cancer.

The earliest identifications of SCCs were generally through Ki67 staining or BrdU chasing[5,6]. These methods are mostly destructive and cannot obtain live cells for subsequent culture or analysis. Label retaining is a common method that can obtain live SCCs. It has been used in research of adult stem cells from normal tissue, like skin, bone marrow, intestine, or breast. Cells from normal tissue or tumor tissue are uniformly labeled with a certain fluorescent dye, and then go through a long period of chasing. Theoretically, fluorescent label will distribute equally into two daughter cells during mitosis. As for SCCs, they will retain more fluorescent labels after multiple mitosis, which were also called as label retaining cells (LRCs). There are many types of fluorescent dyes or fluorescent markers that can be used for label retaining (Fig. 1a, b). Pece et al. utlized lipophilic fluorescent dye PKH26 to label and isolate human normal mammary stem cells and breast cancer stem cells. They found that poorly differentiated tumors showed higher levels of PKH26-retained cells than well-differentiated tumors[7]. Ebinger et al. labeled patient-derived xenografts of acute

lymphoblastic leukemia (ALL) with a protein covalent binding dye CFSE, and identified a group of rare, long-term dormant cells that are chemo-resistant and stemness. Gene expression profile revealed their similarity with primary ALL cells isolated from patients at minimal residual disease[8]. Puig et al. adapted a tetracycline regulated H2B-eGFP fusion protein to label SCCs in Colorectal carcinoma, melanoma, and glioblastoma. They further demonstrate the TET2 is a key regulator of SCCs in cell number, survival, and tumor recurrence[9]. There are many cases where label retaining methods were used to study adult stem cells or cancer stem cells. However, there are still no reports on whether different label retaining methods would result in the same or different population of SCCs. In addition, there still lacks detailed reports on cellular dormancy mechanism in breast cancer, especially triple-negative breast cancer[10,11].

In this study, we utilized three different label retaining methods to simultaneously label MDA-MB-231 cells. After long-term chasing, we found that different fluorescent labels enriched overlapping but non-identical slow cycling cells. We examined the similarities and differences among the three subpopulations of slow cycling cells from many aspects, such as cell cycle, detoxification, and drug resistance. Then we performed RNA-seq to investigate the source of the heterogeneity among the three subpopulations of slow cycling cells. We found that the three subpopulations of slow cycling cells all overexpress AP-1 related genes, and this high expression of AP-1 gene is related to the poor prognosis of TNBC. Through molecular studies, we found the over expression of JunB can directly activate the expression of genes such as *CDKN1A* and *GADD45A*, leading to cell cycle arrest and cellular dormancy. Finally, CC-930, an upstream inhibitor of AP-1, can be combined with chemotherapy drugs to achieve better therapeutic effects.

Results

Different label strategy identified overlapping but not identical slow cycling

cells

To identify SCCs in TNBC, we utilized different fluorescent dyes to label and enrich LRCs. We used PKH26 and Claret which are lipophilic and bound to lipid bilayer structure, as well as CFSE and Violet which covalently bound to intracellular proteins. MDA-MB-231 cells and SUM159 cells were labeled with these dyes separately. After 12 days of chasing, all four fluorescent dyes were found to be able to label and enrich SCCs (Fig. 1c-f and Supplementary Fig. 1). Since each fluorescent dye could label and enrich SCCs, we wondered whether different labeling dyes would enrich different subpopulations of SCCs. We labeled MDA-MB-231 cells and SUM159 cell with the four dyes mentioned above simultaneously and compared SCCs subpopulations with each other. Unsurprisingly, PKH26 label and Claret label had good correlation, even after 12 days of chasing, PKH26 enriched SCCs and Claret enriched SCCs still displayed high correlation. Similar results were also found between CFSE and Violet enriched cells. However, the correlation between cells labeled with different types of dyes wasn't good at first, and decreased fast during 12 days of chasing, indicating heterogeneity existed among SCCs labeled with different types of dyes (Supplementary Fig. 2).

Subsequently, we utilized another fluorescent labeling to obtain a third subpopulation of SCCs. Enhanced green fluorescent protein (eGFP) were fused with Histone 2B and driven by tetracycline response element. When doxycycline was supplied in the culture environment, H2B-eGFP fusion protein was expressed and labeled the nuclei[9] (Fig. 1g, h). It was a firm label due to the long half-life of H2B. After long period of chasing like other fluorescent dyes, we identified another subpopulation of SCCs. To study the heterogeneity of different subtypes of SCCs, we labeled Tet-on stable transfected MDA-MB-231 cells and SUM159 cells with lipophilic dye Claret and protein affinity dye Violet (Fig. 1i, j). After 12 days of chasing, we found more overlapping between H2B-eGFP enriched SCCs and Violet enriched SCCs, while Claret enriched SCCs shared less overlapping with other two subpopulation (Fig. 1k and Supplementary Fig. 3). However, there still existed a small population of cells

retained Claret, H2B-eGFP, and Violet label at the same time, even after 12 days of chasing (Fig. 1l). This rare subpopulation suggested a common origin of different SCCs.

Common phenotypes of SCCs: cell cycle arrested and more stemness

With three diverse subpopulations of SCCs identified, we wondered the similarities and differences in gene expression and phenotype among them. We firstly examined the cell cycle of those cells. qPCR showed that three subpopulation of SCCs shared similar gene expression pattern of cell cycle related genes. Genes in Cip/Kip family, including *CDKN1A*, *CDKN1B*, *CDKN1C* were obviously up regulated, and *CDKN2C* was down regulated. Most cyclin dependent kinases, including *CDK1*, *CDK2* and *CDK6* were down regulated. Most cyclins, including *Cyclin E1*, *Cyclin E2*, *Cyclin A2*, *Cyclin B1* were down regulated as well. Conversely, *CDK4* and *Cyclin D1* had a up regulated tendency (Fig. 2a). Cell proliferation associated genes *MKI67* and *PCNA* were down regulated in all three subpopulations of SCCs, and immunofluorescence showed that H2B-eGFP enriched SCCs had lower expression of Ki67 and p-H3 (Fig. 2b), indicating that most of those cells were arrested in the G1 phase of mitosis.

We next utilized a FastFUCCI system to check cell cycle phase of each individual cells. In eukaryotic cells, licensing factor CDT1 peaked in G1 phase, and underwent a sudden drop in S phase. Its inhibitor, Geminin had a high expression level during S phase and G2 phase, but lowered during late mitosis and G1 phase. Alternate expression of these two proteins were controlled by the alternate activation of E3 ubiquitin ligase SCF^{Skp2} and APC/C^{Cdh1}. Fluorescence ubiquitin cell cycle indicator (FUCCI) technology utilized fluorescent protein mKO and mAG fused to the destabilized sequence of SCF^{Skp2} and APC/C^{Cdh1} respectively, offering accurate means to monitor cell cycle of individual cells[12,13]. FUCCI analysis showed that majority of Claret enriched SCCs and Violet enriched SCCs were arrested in the G1 phase (Fig. 2c). Unlike each other, Violet enriched SCCs rarely entered S phase or G2/M phase (about 10%), while nearly 30% Claret enriched SCCs entered S phase

and G2/M phase. Taken these data together, we could conclude that these three subpopulations of SCCs were dormant and arrested in the G1 phase.

We intended to performed PI staining to validate SCCs' cell cycle arrest, but surprisingly we found a large number of abnormal polyploid cells existed in all three subpopulations of SCCs, especially in Violet enriched SCCs (Fig. 2d). It could be easily understood that abnormal polyploid cells usually expressed more proteins compared with normal diploid cells and mitotic tetraploid cells, thus make them retained more protein affinity Violet dye.

Some particular cancer stem cells (CSCs) had been reported to be dormant[14]. To investigate the relationship between SCCs and CSCs, we utilized Aldeflour to characterize BCSC. We found that $ALDH^+$ cells were more abundant in Claret enriched SCCs and Violet enriched SCCs, compared with bulk cells. Moreover, $ALDH^+$ cells are more abundant in Violet enriched SCCs, compared with Claret enriched SCCs (Fig. 2f). Meanwhile, we found more Claret enriched SCCs and Violet enriched SCCs in $ALDH^+$ cells compared with bulk cells, but the change was not obvious (1.30 % Claret enriched SCCs and 1.70 % Violet enriched SCCs found in $ALDH^+$ cells, compared with ~ 1% of each SCCs found in bulk cells, Supplementary Fig. 4a). We also employed senescence-associated β-galactosidase (SA-β-GAL) staining to detect correlation between SCCs and senescent cells. We found few senescent cells in SCCs, which means three subpopulations of SCCs we identified were not senescent cells with irreversible growth arrest (Supplementary Fig. 4b, c).

Finally, we utilized transwell to detect migration and invasion capacity of SCCs. We found that Claret enriched SCCs had enhanced mobility. H2B-eGFP enriched SCCs and Violet enriched SCCs had more mobility than bulk cells, but the difference was not significant (Fig. 2e and Supplementary Fig. 4d). Taken these data together indicated Claret enriched SCCs were trend to be mesenchymal-like SCCs with high invasive capacity.

Different subpopulations of SCCs had diverse chemo-resistance

Subsequently, we investigated the chemo-resistance of three subpopulations of SCCs to different chemotherapeutic drugs. We chose 13 chemotherapeutic drugs, belonging to three major types of chemotherapeutic drugs: taxanes, anthracyclines and other DNA damage regents, which mainly included three types of drugs currently used in clinical treatment of TNBC (Fig. 3a). We found that three subpopulations of SCCs exhibited different drug resistance after 3 days of treatment. Firstly, all three subpopulations of SCCs exhibited taxanes-resistance, while Violet enriched SCCs were more resistant compared with others (Fig. 3b). Secondly, all three subpopulations of SCCs exhibited anthracyclines-resistance, while H2B-eGFP enriched SCCs were more resistant compared with others (Fig. 3c). Furthermore, Claret enriched SCCs were less chemo-resistance compared with other two subpopulations, which align with our previous data that Claret enriched SCCs had weaker detoxication capacity. Additionally, three populations of SCCs were more resistant to PARP inhibitor olaparib and veliparib, ATM inhibitor CP-466722, but were more sensitive to ATR inhibitor AZD6738 (Fig. 3d and Supplementary Fig. 5). qPCR analyses showed that ATR pathway was down regulated in three subpopulations of SCCs, but *ATM* and *CHEK2* were up regulated (Fig. 3e), which may explain the source of different drug sensitivities. Since SCCs were deficiency in ATR pathway, which makes them more sensitive to ATR inhibitors. These data suggested SCCs were resistant to chemotherapeutic drugs, and different subpopulation of SCCs had heterogeneous drug resistance. But it's also important to note that it was a single dose trial and didn't normalize with cell viability. Ratio of SCCs residual might rise with increasement of dosage.

Different subpopulations of SCCs share similar gene expression pattern

To further explain heterogeneity among different subpopulations of SCCs, we performed bulk RNA-seq with each population of SCCs and ungated bulk cells sorted with FACS (Fig. 4a). Firstly, Pearson correlation analysis showed higher correlations

among three subpopulations of SCCs (Fig. 4b). KEGG pathway analysis showed up regulation of MAPK signaling pathway and PI3K-AKT signaling pathway in three SCCs subpopulations, while down regulated pathways were mainly focus on DNA replication, DNA damage repair, cell cycle and cell cycle checkpoints (Fig. 4c-d). Deficiency in these down regulated pathways consistent with dormant phenotype, and also explain SCCs' sensitivity to PARP inhibitor. Reactome pathway analysis showed similar results with KEGG enrichment in the down regulated genes, and also showed enriched senescence-associated secretory phenotype (SASP) genes in up-regulated genes (Fig. 4c-d).

In addition, we found several bZIP family genes, especially subunits of AP-1, including *FOS*, *FOSB*, *JUN*, *JUNB* and *JUND*, were up regulated in SCCs (Fig. 4e). DNA damage inducible transcripts (DDIT) including *GADD45A*, *GADD45B*, *DDIT3*, *DDIT4* were up regulated in SCCs. CCAAT/Enhancer Binding Protein (C/EBP) family genes *CEBPB* and *CEBPG* were upregulated in SCCs, and *CEBPA* and *CEBPD* were down-regulated in Claret enriched SCCs (Supplementary Figure 8). In another set of RNA-seq, we also found upregulations of AP-1 subunits in PKH26 enriched SCCs (Fig. 4f, 4h). Besides, *FOS* and *FOSB* were the most upregulated genes (Fig. 4g), which indicates that AP-1 might be a key regulator of TNBC cellular dormancy.

we first validated the expression of AP-1 subunits in three subpopulations of SCCs by qPCR (Fig. 5a). Data showed that c-Fos family genes FOS, FOSB and c-Jun family genes JUN, JUNB and JUND were up regulated in all three subpopulations.

Upregulation of AP-1 subunits in TNBC is a predictor of poor prognosis

To investigate correlation between AP-1 subunits' expression and TNBC patients' survival, AP-1 subunits' expression levels were classified into high and low levels via a

cutoff of the median gene expression in TCGA-BRCA cohort. Firstly, we found that TNBC patients with high expression of *FOS* or *FOSB* showed worse overall survival (Fig. 5b, c). We also examined overall breast cancer patients and found non-significant difference in overall survival between the high and low expression of *FOS* or *FOSB*. Since ER status is the most critical factor for survival of BC patients[15], we wondered if the association between high expression of *FOS* or *FOSB* and poor prognosis is ER status related. We found high expression of *FOS* or *FOSB* led to poor prognosis in ER negative patients, but had no influence in ER positive patients (Supplementary Fig. 7a). In addition, we also found a group of TNBC patients with simultaneous high expression of *FOS* and *FOSB*. These patients had worse prognosis compared with others (Fig. 4d-f). We verified our findings in METABRIC-TNBC database (Supplementary Fig. 7b). These data showed that upregulation of *FOS* or *FOSB* is a TNBC specific predictor of poor prognosis.

AP-1 regulate TNBC cellular dormancy and chemo-resistance

To further investigate the mechanism of AP-1 subunits' up regulation affecting cellular dormancy, we utilized an in vitro chemo-treatment model to test whether inhibition of AP-1 could reduce TNBC's chemo-resistance caused by SCCs. We employed a combination of docetaxel, doxorubicin, and cyclophosphamide, with common clinical dosage. We named this combination as TAC for short in the next contents. After 3 days of TAC treatment, remaining cells were collected. We found that all three subpopulations of SCCs increased after TAC treatment, from each population took up ~1% to 6.17 ± 0.44 %, 50.63 ± 0.80 %, 8.88 ± 0.51 %, respectively. Among which H2B-eGFP enriched SCCs showed the most obvious increase, which can be inferred that doxorubicin played a more important role in the enrichment of SCCs. Subsequently, we chose two AP-1 related small molecule inhibitor, CC-930, a selective c-Jun N-terminal kinase (JNK) inhibitor[16], and T-5224, a c-Fos/c-Jun DNA binding inhibitor[17]. By treating MDA-MB-231 cells with two inhibitors in combination with TAC, we found that CC-930 reduced the enrichment of SCCs arising from TAC

treatment, decreased to 5.27 ± 0.27 %, 18.13 ± 0.42 %, 7.74 ± 0.38 % respectively. On the contrary, T-5224 did not reduce this enrichment, rather increased H2B-eGFP enriched and Violet enriched SCCs population up to 61.90 ± 0.46 % and 10.01 ± 0.20 % (Fig. 6a and Supplementary Fig. 8). Moreover, by driven firefly luciferase expression under AP-1 response element, we constructed a dual-luciferase assay to detect AP-1 transcription activity. After 24 hours treatment of CC-930, relative firefly luciferase activity reduced, while T-5224 treatment cells had no significant change compared with control group (Supplementary Figure 12a). Taken these data together, we could conclude that CC-930 could reduce SCCs enrichment during chemo-treatment, and this reduction was due to AP-1 transcription activity inhibition.

We further investigate both gene expression and protein expression after TAC treatment. qPCR showed that *FOS* and *FOSB* had the most obvious up regulation after TAC treatment, with a 32.12-fold change and 193.50-fold change, respectively. Jun family members including *JUN*, *JUNB*, and *JUND* were also up regulated. Among which, JUNB was the most up regulated, with a 9.54-fold change. Meanwhile, we also detected gene expression changes in Cip/Kip family and GADD45s. We found that genes including AP-1 subunits, Cip/Kip family and GADD45s were up regulated after TAC treatment, which were then reduced via CC-930 treatment (Fig. 6b).

Previous studies have shown that c-Jun had at least two phosphorylation sites in both N-terminal and C- terminal. N-terminal phosphorylation contribute to c-Jun's transcription activity and is phosphorylated by JNK. C-terminal phosphorylation weakens binding affinity between c-Jun dimer and DNA, and is phosphorylated by GSK3 or CKII, which is inhibited via cascade phosphorylation of ERK and p70-S6[18]. In short, both JNK phosphorylation and ERK phosphorylation both contribute to AP-1 transcriptional activity. Therefore, we also performed Western Blot detection on MDA-MB-231 cells treated with TAC or combined with CC-930. We found up-regulation in both JNK and ERK's phosphorylation level after TAC treatment, and could be reversed by CC-930.

It's also worth noticing that, although *FOS* and *FOSB* gene expression had most

obvious up regulation after TAC treatment, but there was no corresponding increase in protein level. Instead, the protein level of c-Fos, FosB were down regulated after TAC treatment, along with c-Jun (Fig. 6c). It has been reported that c-Fos is a very unstable protein with rapid nuclear turnover, like other AP-1 subunits[19]. We speculated that this contradiction was caused by rapid degradation of c-Fos and FosB due to the lack of suitable heterodimer ligand after TAC treatment. It also suggested that JunB could form homodimer or heterodimer without helping of c-Jun.

To verify our speculation, we labeled MDA-MB-231 cells with H2B-eGFP and chased for 12 days to perform IF and test the co-localization of c-Jun, JunB and SCCs. We found co-localization between JunB expression, p21,GADD45A and SCCs marker H2B-eGFP (Fig. 6d). Also, we didn't find much expression of c-Jun in SCCs, which suggested that SCCs lacked expression of c-Jun, resulting in rapid degradation of c-Fos and FosB. And it also suggested JunB could form stable dimer without c-Jun.

We further constructed another lentivirus AP-1 reporter system, with mCherry driven by AP-1 response element. Stable transected MDA-MB-231 cells were labeled with Claret, H2B-eGFP and Violet as described above, and chased for 12 days as well. After chasing, AP-1 transcription activity in each subpopulation of SCCs was indicated by mCheery fluorescence intensity. Not only did we find stronger AP-1 transcription activity in SCCs, but we also found transcriptional activity of AP-1 in different subpopulation of SCCs was various. mCherry fluorescence intensity was most robust and specific in Violet enriched SCCs, then H2B-eGFP enriched SCCs and Claret enriched SCCs (Fig. 6e). Immunofluorescence identified co-localization between AP-1 derived mCherry expression and H2B-eGFP (Fig. 6f). It was worth noticing that AP-1 differed little in expression, but varied greatly in function, in three subpopulations of SCCs. It may explain why Claret enriched SCCs did not respond well to CC-930. It may also explain the root of heterogeneity among three subpopulations of SCCs. All these evidence showed that AP-1 is involved in the regulation of cellular dormancy in TNBC, and Inhibition of AP-1 could force SCCs out of dormant state.

JUNB regulate TNBC cellular dormancy though direct activation of CDKN1A and GADD45A

To shed further light on the molecular mechanism of AP-1 regulating TNBC dormancy, we focused on the molecular function of JunB. AP-1 subunits are mainly made up of c-Jun family and c-Fos family. As the active center of AP-1, c-Jun could form homodimer and initiate transcription. c-Fos could form heterodimer with c-Jun, which have more transcriptional activity than the c-Jun homodimer. Both c-Jun homodimer and c-Fos/c-Jun heterodimer was found to promote cell proliferation. While JunB and JunD, especially JunB, were found to form heterodimer with c-Jun, having higher affinity compared with c-Fos. c-Jun/JunB heterodimer has been reported to antagonize c-Jun medicated cell proliferation. In addition, the heterodimer formed by JunB and c-Jun did not only inactivate AP-1, but also can activate the expression of some particular genes[18,20]. Considered that JunB is a negative regulator of AP-1 and also up regulated in both SCCs and after TAC treatment, we focused our interest on how JunB regulate TNBC cellular dormancy.

We extracted promoter region sequences of Cip/Kip family and GADD45s and analyzed with JASPAR database. We found that AP-1 binding site commonly existed in the promoter region of Cip/Kip family and GADD45s. Among which, higher affinity was found on both *CDKN1A* promoter and *GADD45A* promoter (Fig. 7a and Supplementary Table 1). We then constructed another dual-luciferase assay by driven firefly luciferase expression under whether *CDKN1A* promoter or *GADD45A* promoter. We compared relative firefly luciferase activity while transfected with whether JunB overexpression vector or control vector. A higher relative firefly luciferase activity was found when JunB overexpression was transfected, indicating high level of JunB directly activated transcription of either *CDKN1A* or *GADD45A* (Supplementary Fig. 9b). Meanwhile, when JunB overexpression vector was co-transfected with former constructed AP-1 response dual-luciferase system, stronger relative firefly luciferase activity was found, indicating overexpression of JunB could initiate AP-1 transcription (Supplementary Fig. 9c).

We obtained MDA-MB-231 cell line with stable overexpressing JunB via lentivirus transfection, and control vector was transfected as well. We found gene expression level of *JUNB*, *FOS*, *FOSB*, *CDKN1A* and *GADD45A* were up regulated in JunB overexpression cells (Fig. 7b). Western blot showed up regulation of p21 and Gadd45a in JunB overexpression cells. Meanwhile phosphorylated Erk1/2 was up regulated (Fig. 7d). We synthesized two siRNA targeting *JUNB* then transfected into MDA-MB-231 cells, and found opposite gene expression pattern with overexpression of JunB. AP-1 subunit *FOS*, *FOSB* and *JUN* were down-regulated, and *CDKN1A*, *CDKN1B*, *GADD45A* and *GADD45B* were also down-regulated (Fig. 7c). All these data suggested c-Jun/JunB heterodimer could transcriptionally activate Cip/Kip family and GADD45s.

To investigate JunB's impact on tumorigenesis, we utilized xenograft either derived from JunB overexpressing cells or control cells. After 21 days of mammry fat pad in situ injection, JunB overexpressing cells derived significant larger xenografts compared with control cells, in both terms of tumor volume and tumor weight (Fig. 7e and Supplementary Fig. 10a). All these evidence showed that up regulation of JunB in SCCs was a major factor contributing to cellular dormancy and tumorigenesis.

CC-930 could reduce SCCs residual after chemotherapy in vivo

To explore the possibility of anti-SCCs therapy for the clinical treatment of TNBC, we examined CC-930's anti-tumor capacity both in vitro and in vivo. In previous experiments, we have demonstrated that CC-930 could reduce the residue of SCCs after chemotherapy. Next, we performed colony formation assay of SCCs compared with bulk cell, cultured with present or absent of CC-930. We found SCCs had more colony formation capacity then bulk cells, and CC-930 could reduce the formation of colonies (Supplementary Fig. 10c).

To further investigate CC-930 anti-SCCs activity in vivo, we established 40 CDX models with both AP1re reporter and H2B-eGFP chasing system. Nude mice bearing CDX were randomly divided into four group, with 21 days treatment of control group,

CC-930 treatment, TAC treatment or TAC + CC-930 combination. Tumors with TAC treatment shrinked at first but relapsed after 14 days. CC-930 treatment along had limited anti-tumor capacity but functioned well when combined with TAC. The combination effectively reduced the size and weight of the tumor, and also prevent the recurrence of the tumor (Fig. 8a-c). Mice body weight had decreased tendency as treatment progresses in TAC and combination group, while did not occur in CC-930 treatment group (Supplementary Figure 10b). It's also worth noting that abdominal metastases were observed in part of tumors in control group and TAC group. Although tumors in CC-930 group relapsed during the last week of treatment and the tumor volume had no significant difference from that of the control group, none of tumors in CC-930 group was observed with abdominal metastases. Similarly, abdominal metastases were significantly reduced in the combination group compared with TAC group (Supplementary Table 2). These data suggested CC-930 could improve survival in TNBC patients treated with traditional chemotherapy.

Discussion

Label retaining is the most common method to label and enrich SCCs, also allows capturing live SCCs for subsequent experiments. Since label retaining method relied on fluorescent labeling, there exist conflict between label retaining dye and other experiment reagent, occasionally. In some cases, drug treatment will also change the fluorescence of cells. To avoid the competition of fluorescent channel, we investigated the heterogeneity of SCCs labeled with different types of fluorescent dyes. We chose the most accessible label dyes, including lipophilic dyes, protein covalent binding dyes and chromatin labeled fluorescent protein. The substances with which these dyes are compatible with match the most common components of cells. We found that the same type of fluorescent dye labeled almost the same population of cells. This finding can well solve the conflict we mentioned earlier. When the fluorescent channel is occupied by other reagents or metabolites produced by drugs, we can choose an alternative dye with the same substrate but different fluorescent channel. In fact,

lipophilic fluorescent dyes or protein covalent binding dyes have various alternatives with different fluorescent channels, and the chromatin labeling method can be replaced by changing the fluorescent protein of H2B fusion, although the latter is relatively inconvenient. As demonstrated in our previous review, application of different types of fluorescent labels has own limitations[21]. After long period of chasing, fluorescence intensity of protein covalent binding dyes was too dim to visualize under microscope. Lipophilic fluorescent dyes had brighter fluorescence to visualize, but may detach from cells undergo surfactant based permeabilization, such as Triton X-100. Taken together, our findings can provide a more comprehensive guide for the selection of fluorescent labels in the study of SCCs.

While in the process of studying the heterogeneity of SCCs labeled with different types of fluorescent dyes, we also found that different types of fluorescent labels tend to enrich overlapping but non-identical SCCs. These SCCs have some similarities in phenotype. For instance, they are all in slow-cycling state and are relatively insensitive to chemotherapeutic drugs. There are also many differences in the phenotypes of SCCs of different subpopulations. Claret enriched SCCs are less chemo-resistant, have more cells out of G1 phase, stronger mobility and more aggressive, with the shortest survival time in animal model. H2B-eGFP and Violet enriched SCCs exhibit enhanced chemo-resistance, stronger detoxification, and have more cells arrested in G1 phase, but weaker migration and invasion capabilities. These differences and similarities conform with the results obtained by flow cytometry tSNE dimensionality reduction, suggesting that Claret enriched SCCs and H2B-eGFP/Violet enriched SCCs have different capacities and status. It is worth noticing that, even after 12 days of chasing, there still exist a small group of cells with simultaneous Claret, H2B-eGFP and Violet dye residual. It is still unknown whether the common SCCs are the progenitor cells of the three subpopulations of SCCs or the intermediate state in the differentiation process of the three subpopulations of SCCs.

Cellular heterogeneity is one of the most important and clinically relevant areas in cancer research, for tumor obtained distinct subsets of cancer cells with diverse

451 morphology, cellular functions, and tumorigenic capacities[22]. To obtain better
452 understand SCCs' function and significance in tumor mass, we inspected and
453 discussed relationship between SCCs and two other heterogenous subpopulation,
454 cancer stem cell and senescent cells. We found more $ALDH^+$ characteristic BCSC in
455 SCCs compared with bulk cells, especially in Violet enriched SCCs. This result seems
456 to be contrary to the previous conclusion that $ALDH^+$ characteristic BCSCs are in the
457 proliferation state[23]. Since SCCs only comprise a small fraction of bulk cells and
458 ALDH+ cells, it does not conflict with fact that most $ALDH^+$ characteristic BCSCs are
459 in the proliferation state. We also noticed Violet enriched SCCs with higher ALDH
460 function had limited invasive capacity compared with Claret enriched SCCs, which
461 was consistent with previous reports[23]. We found several senescent markers
462 expressed in SCCs, including mitotic arrest, without doubt, and enlarged and flattened
463 morphology, activation of SASP, and irregular polyploid[24]. But we also found that
464 overwhelming majority of SCCs were SA-β-GAL negative. The most recent review of
465 hallmarks of cancer argued senescent cell is a functionally important cell types in
466 tumor microenvironment[25]. Three modes of senescence are distinguished by the
467 origin of stasis: replicative senescence, oncogene-induced senescence, and
468 therapy-induced senescence. In contrast to the previous definition, some senescent
469 cancer cells are thought to be in a transitory, reversible state of senescence, which
470 could escape of bypass cellular senescence. Even polyploid cells, which are generally
471 considered to be terminally differentiated can restore proliferation capacity through
472 neosis. It has been reported that p38MAPK/p16 pathway generally involved in cell
473 cycle arrest and maintenance of senescence[26]. While some tumors, including
474 MDA-MB-231 are CDKN2A mutated[27], which may allow senescent cancer cells to
475 escape senescence state easier. We considered that SCCs are associated with
476 senescent cells, especially oncogene-induced senescence, and therapy-induced
477 senescence. With existence of external survival pressure, SCCs can not only survive
478 and generate daughter cells to maintain tumor mass, but also play the function of
479 senescent cells to promote tumor initiation and progression and escape immune

recognition.

We conducted RNA-seq experiments to analyze the source of SCC dormancy. We found a similar gene expression pattern across all three subpopulations of SCCs. They were all down regulated in cell cycle, DNA replication, DNA damage repair and other related pathways, and were all up regulated in MAPK pathway and cellular senescence pathway. We found AP-1's function, especially JunB molecular function was a key regulator in cellular dormancy. As a negative regulator in AP-1, JunB could form heterodimer with c-Jun, competing with c-Fos and FosB and inactive them. The c-Jun/JunB heterodimer can also directly activate transcription of genes such as *CDKN1A* and *GADD45A*, thereby blocking the cell cycle. Meanwhile we found some genes such as *FOS* and *FOSB* have high gene expression, but with low protein levels, probably due to degradation caused by lacking dimer formation. This high level of gene expression is beneficial for cells to re-enter cell cycle and proliferate. When the external environment changes, high level of gene expression can be effectively translated to protein, thereby further promoting cell proliferation. This potential is common existent in many stem cells. Finally, we found that CC-930 can sensitize SCCs to chemotherapeutic drugs by inhibiting the activity of AP-1. CC-930 thereby achieving the purpose of further killing tumors and reducing minimal residues and recurrence. We found CC-930 used alone did not have obvious tumor suppressive ability, probably due to CC-930 forced SCCs out of cell cycle arrest and entered into a rapid mitosis state, thus producing more daughter cells and tumor growth. Even so, CC-930 had the capacity to prevent abdominal metastases, and also reduced abdominal metastases caused by TAC treatment in combination group. It's also worth noting that CC-930 is a safe, orally active drug[28]. CC-930 dosage we used in our in vivo assay was related low compared with other CC-930 in vivo assay published before[29–31]. A higher dose of CC-930 may yield better results. Alternatively, the dosage of chemotherapy drugs could be reduced with higher dose of CC-930 to reduce the side effects of chemotherapy and improve the survival and quality of life of TNBC patients. These findings emphasized that anti-SCCs therapy can effectively improve

survival in TNBC patients and that CC-930 is an effective anti-SCCs therapy.

This article also has many limitations as well. First, the heterogeneity of SCCs has only been studied in TNBC, and most models are based on MDA-MB-231 cell line in vitro models, lacking microenvironment and immune infiltration. It's also unknown whether our findings are valid for other types of cancer. Secondly, there lacks well explanation for the source of the differences between SCCs. Mainly because we only utilize gene expression level to explain this heterogeneity. We found AP-1 related genes were up regulated in all three SCCs subpopulations, but AP-1 response indicator demonstrate that AP-1 was inactive in Claret enriched SCCs. This may explain the source of differences between Claret enriched SCCs and other subpopulations. However, the process of AP-1 inactivation in Claret enriched SCCs remains unexplained. To deeper understand the source of heterogeneity in SCCs, more dimensional and higher-precision studies are needed, such as scRNA-seq and scATAC-seq. It also reminds us that for the study of SCCs, it may not be enough to study only one type of SCCs.

Methods

Cell lines and labeling. MDA-MB-231 and SUM159 cells were generous gifts from Dr. Zuoren Yu. HEK293T cell line was a generous gift from Dr. Ke Wei. MDA-MB-231 cells and HEK293T cells were cultured with DMEM medium supplied with 10% FBS, SUM159 cells were cultured with RPMI-1640 medium supplied with 10% FBS (GIBCO). Lentivirus packing was conducted as described before. MDA-MB-231 cells were transfected with lentiviruses and 10 mg/ml polybrene for 24 hours. At least 72 hours after transfection, cells were pelleted and sorted using FACS.

For PKH26 and Claret (Sigma) chasing, cells were washed with PBS 3 times, resuspend with Diluent C solution provided with the kit, and incubated with 10 mM PKH dye for 5 minutes at room temperature, protecting from light. Afterwards, cells were washed with Diluent C solution 3 times, and cultured in complete medium. For CFSE and Violet (Invitrogen) chase, cells were washed with PBS once, resuspend with PBS and incubated with 5 mM CellTrace dye for 20 minutes at 37 ℃, protecting from light. Afterwards, cells were washed with complete medium twice, then cultured in complete medium. For doxycycline (DOX) chase, cells were treated with 5 mg/ml DOX for at least 3 days in advance, then cultured in DOX-free complete medium. For cells labeled with multiple dyes, perform PKH dyes labeling prior to CellTrace dyes labeling, and culture the labeled cells in DOX-free complete medium.

Xenograft model. 4-5 weeks old female nude mice were purchased from JiCui. After one week of adaption, 1 * 10^6 MDA-MB-231 cells resuspended with 50μl PBS and 50μl Matrigel were injected into the fourth mammary fat pad on the right flank. When the tumor volume reached approximately 300 mm^3 at approximately 1 week, the mice were randomly assigned into control group, 4 mg/kg CC-930 group, TAC (5 mg/kg/week docetaxel, 3.33 mg/kg/week doxorubicin, and 33.33 mg/kg/week cyclophosphamide) group and 4 mg/kg CC-930 + TAC group. CC-930 was given to mice orally, on a daily basis for 21 days. TAC was given to mice i.p. once a week. The tumor volume and body weight were measured three times a week until two days after the final treatment. Tumor volume was calculated as 0.5 × $width^2$ × length. Mice were then sacrificed, and tumors were removed, weighted, and fixed for immunohistochemistry.

Plasmids and siRNAs. TetOn-H2BeGFP plasmid (pSIN-TRE-H2BeGFP-hPGK-rtTA2) and fastFUCCI plasmid (pBOB-EF1-FastFUCCI-Puro, Addgene #237968) were provided by xxx.

Homo sapiens JUNB CDS sequence (NCBI Accession No. NM_002229.3) was synthesized and cloned into multiple cloning sites of pLenti-CMV-MCS-mCherry, which was a generous gift from Dr. Ke Wei. Constructed plasmid was named pLenti-CMV-JunB-mCherry and used for JunB ovexpressing. pLenti-CMV-MCS-mCherry was used as a negative control of JunB overexpressing.

pGL3-basic and pRL-SV40 plasmids were generous gifts from Dr. Yandong Li.

AP-1 response element (6x TGAGTCAG) and a minimal TATA-box promoter were synthesized and cloned into pGL3-basic. This constructed plasmid was named pGL3-AP1re and used to detect AP-1 inhibition activity of CC-903 and T5224. Same synthesized sequence was also cloned into pLenti-5'MCS-CMV-mCherry, replaced whole CMV prompter. Constructed plasmid was named pLenti-AP1re-mCherry and used to trace AP-1 activated cells in vitro.

2 kb upstream of transcription initiation site was considered as promoter region. Promoter region of Homo sapiens CDKN1A (NCBI Gene ID: 1026) and GADD45A (NCBI Gene ID: 1647) were synthesized and cloned into pGL3-basic respectively. Constructed plasmid was named pGL3-pCDKN1A and pGL3-pGADD45A, and used to detect JunB's transcriptional activation of both genes.

siRNAs were designed targeting to CTCTCTCTACACGACTACAAA sequence and CATACACAGCTACGGGATA sequence of Homo sapiens JUNB. 200 pmol siRNA was transfected into MDA-MB-231 cells via lipofectamine 2000 (Invitrogen). 48 hours after transfection, cells were collected for subsequent experiments.

All DNA fractions and siRNA were synthesized by Sangon Biotech, Shanghai.

Flow cytometry. For chasing analysis, single dye labeled cells and tri-labeled cells were pelleted and fixed with IC fixation buffer (Invitrogen) every other day from day 0 to day 12.

For cell cycle analysis with PI staining, cells were fixed overnight and washed twice in cold PBS. $1 * 10^6$ cells were resuspended in 500 μl PI/RNAse staining solution (Invitrogen) for 30 minutes in room temperature, protecting from light.

For cell cycle analysis with FUCCI, cells transfected with FUCCI were labeled with Claret and Violet as described above, chased for 12 days and fixed. $1 * 10^4$ cells were collected for each bulk cell group, $1 * 10^6$ cells were collected for each LRCs group.

For ALDEFOUR assay, cells were labeled with Claret and Violet as described above, chased for 12 days without fixation. $1 * 10^6$ cells were resuspended in 1ml Assay buffer provided with the kit (Stemcell), and 5 μl ALDEFLOUR was added for 60 minutes at 37 ℃. Control group was carried out by adding additional 10 μl DEAB, and incubated in the same condition. Cells were washed and resuspended in Assay buffer. $1 * 10^4$ cells were collected for each bulk cell group and DEAB control group, $1 * 10^6$ cells were collected for each LRCs group.

A Beckman cytoflex system was used to collect the fluorescence intensity, and Flow-Jo v10 was used to analysis the data. The t-SNE module was provided by Flow-Jo v10.

For live cell sorting, a Beckman Moflo system was used. Tri-labeled cells were cultured for 12 days, and top 1% population of each dye were sorted by FACS, with ungated bulk cells as reference control.

Reverse transcription and quantitative PCR. To analyze the expression of selected genes in bulk cells and subpopulations of LRCs, tri-labeled cells were cultured for 12

days, and top 1% population of each dye were sorted by FACS, with ungated bulk cells as reference control. Total RNA was extracted using Trizol (Invitrogen) and used to synthesize cDNA using RT reagent Kit with gDNA Eraser, and oligo dT and random hexamer primers were used together (Takara). A Q6 qPCR System was used with TB Green Premix Ex Taq (Takara), and specific pairs of primers (Supplementary Table 3) to detect the indicated transcripts. Relative gene expression was determined by the comparative Ct method.

Immunofluorescence. Tet-on H2BeGFP stabled transfected cells were cultured with DOX for 3 days, chased in DOX-free medium for 12 days, and fixed with 4% PFA. Cells were separated into 4-well chamber slides at least two days before fixation. After fixation, cells were permeabilized with 0.1% Triton X-100 in PBS. Cells were washed twice with PBS and blocked with 4% FBS. Target antibodies were incubated with recommended dilution. Secondary antibody and Hoechst 33342 were stained together. A xxx system was used to collect image.

Western Blot. Cells were pelleted and washed once with PBS and resuspended in RIPA lysis buffer supplied with protease inhibitor and phosphatase inhibitor. An ultrasonic device was used to disrupt cells, and lysates were centrifuged to collect supernatants. Protein concentrations were quantified with BCA, and 100 μg of each component was loaded. Proteins were separated by SDS-PAGE with 5% spacer gel and 12% separating gel, and later transferred to a PVDF membrane. The membrane was blocked with blocking buffer (LI-COR), and targeted antibodies were incubated with recommended dilution. IRDye-conjugated secondary antibodies were used, and images were collected with an Odyssey system. All the washed were performed with TBST.

Transwell assay. Transwell permeable inserts (Corning) were used for migration and invasion analysis. Tri-labeled cells were chased for 12 days, subpopulation of LRCs and ungated bulk cells were sorted by FACS as described above. Cells were washed and resuspended with 200 μl FBS-free DMEM medium, and seeded in the upper chamber of inserts with $2.5 * 10^4$ cells in each well. The inserts used for invasion analysis were coated with 20 mg Matrigel (Corning) in advance. 500 ml complete medium was added to each well of 24-well plate as lower compartment, and the inserts were seated soon after. Continued to culture for 24 hours with migration assay, and 48 hours with invasion assay. The inserts were fixed with 1% crystal violet solution for 30 minutes and washed twice with ultrapure water. Cells were counted under microscope with 5 sights for each insert.

In vitro and in vivo chemoresistance. For in vitro chemoresistance assay, tri-labeled cells were chased for 9 days, and 1 μM of each drug (TargetMol.USA) were added. Cells were incubated for 72 hours before fixation and analysis with FACS. For anti-AP1 and TAC combination assays, tri-labeled cells were chased for 9 days prior to drug treatment. A combination of 1.867 μM docetaxel, 1.724 μM doxorubicin, and

35.829 μM cyclophosphamide (TargetMol.USA) was named as TAC. 10 μM CC-930 or T-5224 (TargetMol.USA) were used solo or in combination with TAC. Cells were incubated for 72 hours before fixation and analysis with FACS. Cells used for RT-qPCR analysis and Western Blot analysis didn't need to be labeled in advance.

For in vivo drug treatment, CC-930 was first dissolved in DMSO at 20 mg/ml, then diluted with sterile water. Docetaxel, doxorubicin, and cyclophosphamide was dissolved in DMSO at 50 mg/ml, 66.67 mg/ml and 55.55 mg/ml respectively. One volume of docetaxel, two volume of doxorubicin and twelve volumes of cyclophosphamide were mixed into TAC. Before injection, TAC was diluted 20 times with 30% PEG-300, 5% Tween-80 and 60% sterile water.

Dual luciferase assay. To determine CC-930 and T-5224's inactivation effect on AP-1, pGL3-AP1re was construct as described above. 2500 ng pGL3-AP1re and 25 ng pRL-SV40 were transfected into HEK293T cells. 24 hours after transfection, 10 μM of CC-930 and T-5224 were added respectively, and equivalent DMSO was used as control. After 72 hours of treatment, mediums were removed, and lysis buffer was added and shook gently for 15 minutes. The lysates were centrifuged, and 100 ml supernatants were added into white 96-well plate. Both Firefly luciferase activity and Renilla luciferase activity were measured with Glo/Max luminometer following the manual.

To determine JunB activation effect of AP-1, a combination of 1250 ng pLenti-CMV-MCS-mCherry or pLenti-CMV-JunB-mCherry, 1250 ng pGL3-baisc or pGL3-AP1re, and 12.5 ng pRL-SV40 were transfected into HEK293T cells. After 72 hours of transfection, cell lysis and luciferase activity measurements were performed as described above.

To determine JunB activation of CDKN1A and GADD45A transcription, a combination of 1250 ng pLenti-CMV-MCS-mCherry or pLenti-CMV-JunB-mCherry, 1250 ng pGL3-baisc or pGL3-pCDKN1A or pGL3-GADD45A, and 12.5 ng pRL-SV40 were transfected into HEK293T cells. After 72 hours of transfection, cell lysis and luciferase activity measurements were performed as described above.

Relative luciferase activity was calculated using Firefly luciferase luminous intensity / Renilla luciferase luminous intensity (Luc/RLuc) and normalized with control group.

Colony formation. 500 FACS sorted cells were plated in 12-well plate and cultured with 500 ml complete medium overnight. 1μM CC-930 or equivalent DMSO were added, and half medium were replaced every three days. After 12 days of culture, cells were washed with PBS twice and stained with 1% crystal violet solution for 30 minutes and washed twice with ultrapure water. Images were obtained with Bio-Rad xxx system.

SA-β-GAL staining. FACS sorted cells were plated in 4-well chamber slide and cultured overnight. Cells were washed with PBS once and fixed with 500 μl β-Galactosidase fixation buffer (Beyotime). After fixation, cells were washed with PBS

for 3 minutes for 3 times, and stained with 500 μl mix working staining solution supplied with the kit at 37 ℃ overnight. Images were obtained with xxx system.

RAN-seq. Cell were chased and sorted, and RNA was extracted as described above.

Survival.

Statistical analysis. Statistical analyses were performed using GraphPad Prism software or using R. In general, student's *t*-test, paired or unpaired two-tailed *t*-test were used to calculate the statistical significance between comparisons depending on the data type. $P<0.05$ is considered statistically significant.

Data availability

The RNA-seq data have been deposited in GEO database under accession code

References

1. Sung, H. *et al.* Global Cancer Statistics 2020: GLOBOCAN Estimates of Incidence and Mortality Worldwide for 36 Cancers in 185 Countries. *CA. Cancer J. Clin.* **71**, 209–249 (2021).
2. Feng, Y. *et al.* Breast cancer development and progression: Risk factors, cancer stem cells, signaling pathways, genomics, and molecular pathogenesis. *Genes Dis.* **5**, 77–106 (2018).
3. Davis, J. E., Kirk, J., Ji, Y. & Tang, D. G. Tumor Dormancy and Slow-Cycling Cancer Cells. *Adv. Exp. Med. Biol.* **1164**, 199–206 (2019).
4. Gomis, R. R. & Gawrzak, S. Tumor cell dormancy. *Mol. Oncol.* **11**, 62–78 (2017).
5. Naumov, G. N. *et al.* Persistence of solitary mammary carcinoma cells in a secondary site: a possible contributor to dormancy. *Cancer Res.* **62**, 2162–2168 (2002).
6. Li, L. & Clevers, H. Coexistence of quiescent and active adult stem cells in mammals. *Science* **327**, 542–545 (2010).
7. Pece, S. *et al.* Biological and Molecular Heterogeneity of Breast Cancers Correlates with Their Cancer Stem Cell Content. *Cell* **140**, 62–73 (2010).
8. Ebinger, S. *et al.* Characterization of Rare, Dormant, and Therapy-Resistant Cells in Acute Lymphoblastic Leukemia. *Cancer Cell* **30**, 849–862 (2016).
9. Puig, I. *et al.* TET2 controls chemoresistant slow-cycling cancer cell survival and tumor recurrence. *J. Clin. Invest.* **128**, 3887–3905 (2018).
10. Quayle, L. A., Ottewell, P. D. & Holen, I. Chemotherapy resistance and stemness

in mitotically quiescent human breast cancer cells identified by fluorescent dye retention. *Clin. Exp. Metastasis* **35**, 831–846 (2018).

11. Quayle, L. A., Spicer, A., Ottewell, P. D. & Holen, I. Transcriptomic Profiling Reveals Novel Candidate Genes and Signalling Programs in Breast Cancer Quiescence and Dormancy. *Cancers* **13**, 3922 (2021).
12. Koh, S.-B. *et al.* Quantitative FastFUCCI assay defines cell cycle dynamics at single-cell level. *J. Cell Sci.* jcs.195164 (2016) doi:10.1242/jcs.195164.
13. Zielke, N. & Edgar, B. A. FUCCI sensors: powerful new tools for analysis of cell proliferation: FUCCI sensors. *Wiley Interdiscip. Rev. Dev. Biol.* **4**, 469–487 (2015).
14. Qin, J. *et al.* The PSA−/lo Prostate Cancer Cell Population Harbors Self-Renewing Long-Term Tumor-Propagating Cells that Resist Castration. *Cell Stem Cell* **10**, 556–569 (2012).
15. Kast, K. *et al.* Impact of breast cancer subtypes and patterns of metastasis on outcome. *Breast Cancer Res. Treat.* **150**, 621–629 (2015).
16. Plantevin Krenitsky, V. *et al.* Discovery of CC-930, an orally active anti-fibrotic JNK inhibitor. *Bioorg. Med. Chem. Lett.* **22**, 1433–1438 (2012).
17. Ishida, M. *et al.* T-5224, a selective inhibitor of c-Fos/activator protein-1, improves survival by inhibiting serum high mobility group box-1 in lethal lipopolysaccharide-induced acute kidney injury model. *J. Intensive Care* **3**, 49 (2015).
18. Meng, Q. & Xia, Y. c-Jun, at the crossroad of the signaling network. *Protein Cell* **2**, 889–898 (2011).

19. Vesely, P. W., Staber, P. B., Hoefler, G. & Kenner, L. Translational regulation mechanisms of AP-1 proteins. *Mutat. Res. Mutat. Res.* **682**, 7–12 (2009).

20. Hess, J. AP-1 subunits: quarrel and harmony among siblings. *J. Cell Sci.* **117**, 5965–5973 (2004).

21. Basu, S., Dong, Y., Kumar, R., Jeter, C. & Tang, D. G. Slow-cycling (dormant) cancer cells in therapy resistance, cancer relapse and metastasis. *Semin. Cancer Biol.* (2021) doi:10.1016/j.semcancer.2021.04.021.

22. Liu, X. *et al.* Systematic dissection of phenotypic, functional, and tumorigenic heterogeneity of human prostate cancer cells. *Oncotarget* **6**, 23959–23986 (2015).

23. Liu, S. *et al.* Breast Cancer Stem Cells Transition between Epithelial and Mesenchymal States Reflective of their Normal Counterparts. *Stem Cell Rep.* **2**, 78–91 (2014).

24. De Blander, H., Morel, A.-P., Senaratne, A. P., Ouzounova, M. & Puisieux, A. Cellular Plasticity: A Route to Senescence Exit and Tumorigenesis. *Cancers* **13**, 4561 (2021).

25. Hanahan, D. Hallmarks of Cancer: New Dimensions. *Cancer Discov.* **12**, 31–46 (2022).

26. Spallarossa, P. *et al.* p38 MAPK and JNK antagonistically control senescence and cytoplasmic p16INK4A expression in doxorubicin-treated endothelial progenitor cells. *PloS One* **5**, e15583 (2010).

27. Bamford, S. *et al.* The COSMIC (Catalogue of Somatic Mutations in Cancer)

database and website. *Br. J. Cancer* **91**, 355–358 (2004).

28. Macias, H. & Hinck, L. Mammary gland development: Mammary gland development. *Wiley Interdiscip. Rev. Dev. Biol.* **1**, 533–557 (2012).

29. van der Velden, J. L. J. *et al.* JNK inhibition reduces lung remodeling and pulmonary fibrotic systemic markers. *Clin. Transl. Med.* **5**, 36 (2016).

30. Reich, N. *et al.* Jun N-terminal kinase as a potential molecular target for prevention and treatment of dermal fibrosis. *Ann. Rheum. Dis.* **71**, 737–745 (2012).

31. Yang, F. *et al.* c-Jun Amino Terminal Kinase Signaling Promotes Aristolochic Acid-Induced Acute Kidney Injury. *Front. Physiol.* **12**, 599114 (2021).

Acknowledgements

We acknowledge the support of xxx. We apologize to the colleagues whose work was not cited due to space constraint.

Author contributions

Y.D., J.Z. and D.T. conceived and designed the study, interpreted data, and finalized the manuscript;

Y.D. performed most experiments;

J.B. conducted Bioinformatic analysis, and provided assistance in graphic processing and manuscript writing;

R.F. provided assistance in flow cytometry sorting and analysis;

H.S. and S.W. provided assistance in animal experiments;

All authors read and approved the manuscript.

Competing interests: The authors declare no competing interests.

Additional Information

Supplementary Information is available for this paper at https://doi.org/.....

Fundings: This study was supported by the Chinese Ministry of Science and Technology (MOST) Grant (2016YFA0101201)

Reprints and permission information is available online at:

Publisher's note:

Figure Legend

Fig 1: Different LRC strategies identify overlapping but non-identical SCC populations.

(a,b)MDA-MB-231 cells and **(c,d)** SUM159 cells were labeled with PKH26, Claret, CFSE, and Violet separately. Cells were fixed every other day from day 0 to day 12.

(e) Timeline of label retaining strategies. Stable transfected MDA-MB-231 cells were cultured with doxycycline for at least 3 days, then claret labeling and violet labeling were accomplished in order.

(f) Schematics of Tet-On H2B-eGFP expression vector.

(g,h) Label retaining effect of Claret, H2B-eGFP and Violet in tri-labeled cells.

(i) tSNE plot and **(j)** stacked histogram of each time point.

Fig 2: Biological and functional properties of SCCs

(a) 3 SCCs populations showed similar gene expression pattern in cell cycle related genes. Relative gene expressions of FACS sorted SCCs and bulk cells were analyzed by RT-qPCR.

(b) Immunofluorescence showed H2B-eGFP enriched SCCs had lower expression of p-H3 and Ki67 after 12 days of chasing. Scale bar = 20 μm.

(c) Cell cycle of each population was monitored by FUCCI. Claret+ featured LRCs were spread among different phases, while Violet+ featured LRCs were mostly arrested in late G1 phase.

(d) Transwell assay demonstrated SCCs had higher mobility and invasiveness, especially Claret enriched SCCs. Data are represented as mean ± SEM.

(e) ALDH+ cells were more enriched in SCCs compared with bulk MDA-MB-231 cells.

Data are represented as mean ± SD except transwell assay. *p ≤0.05; **p ≤0.01; ***p ≤0.001, Student's t test.

Fig 3: Diverse SCCs have different chemotherapeutic tolerances

(a) Timeline of chemo-resistance assay. Tri-labeled MDA-MB-231 were chased for 9 days, and 1 mM each drug was added respectively. After 3 days of culture cells were collected and analyzed with flow cytometry.

(b) Violet enriched SCCs were more insensitive to taxanes.

(c) H2B-eGFP enriched SCCs were more insensitive to anthracyclines.

(d) SCCs were more sensitive to ATR inhibitor AZD6738.

(e) SCCs were up-regulated in *ATM* and *CHEK2*, and down-regulated in ATR pathway.

Data are represented as mean ± SD. *p ≤0.05; **p ≤0.01; ***p ≤0.001, Student's t test.

Fig 4: RNA-seq reveal SCCs are enriched in AP-1 signaling and anti-stress proteostasis mechanisms

(a) Flow chart of FACS and RNA-seq. Tri-labeled MDA-MB-231 were chased for 12 days. Top 1% of each population were sorted and names as distinct SCCs subpopulation. Meanwhile, cells that were not gated with any fluorescence channel were sorted as Bulk

cell control. Each subpopulation was collected for one sample.

(b) Person correlation showed 3 subpopulations of SCCs were similar to each other in gene expression level.

(c) GSVA analysis showed similar pathway enrichment in three SCCs subpopulations.

(d) GSEA analysis showed MAPK signaling pathway and PI3K-AKT signaling pathway were up-regulated in SCCs, and cell cycle and DNA replication associated pathways were down-regulated in SCCs.

(e) SCCs were enriched in AP-1 subunits' gene expression.

(f) Flow chart of FACS and RNA-seq. MDA-MB-231 cells were labeled and chased with PKH26 for 12 days. Top 1% PE^+ cells were sorted and named as SCCs, and PE^- cells were sorted and names as RCCs. Each subpopulation was collected with triple replications.

(g) FOS and FOSB were the most remarkable up-regulations genes in SCCs.

(h) AP-1 complex were up-regulated in SCCs.

(i) High expression level of *FOS* was poor prognostic factor for TNBC patients. Patients with both gene expression > median were considered as high-expression group. Data was acquired from TCGA-BRCA database. n = 111 each, total n =222.

(j) TNBC patient with both *FOS*/*FOSB* high expression had worse prognosis. Patients with both *FOS*/*FOSB* gene expression > median gene expression were considered as high-expression group. Data was acquired from TCGA-BRCA database. n=80, total n=222.

Fig 5: Mechanisms of AP-1-mediated anti-stress signaling in regulating TNBC SCC properties

(a) SCCs were enriched in AP-1 subunits in mRNA level. Relative gene expressions of FACS sorted SCCs and bulk cells were analyzed by RT-qPCR. Data are represented as mean ± SD. **(b)** JunB, p21 and GADD45A were enriched in H2B-eGFP enriched SCCs after 12 days of chasing. Scale bar = 20 μm.

(c) CC-930 could reduce SCCs residual caused by chemotherapy in vitro. TAC was a combination of docetaxel, doxorubicin, and cyclophosphamide, with common clinical dosage. Data are represented as mean ± SD.

(d) mCherry were expressed via AP1RE to construct AP-1 transcriptional activity reporter system. AP-1 promoted mCherry and SCCs marker H2B-eGFP were co-localized after 12 days of chasing. Scale bar = 20 μm.

(e) SCCs had higher AP-1 transcriptional activity, and Violet enriched SCCs' was most robust.

(f-g) CC-930 could reduce gene expression and protein level upregulated by TAC treatment. MDA-MB-231 cells were treated with TAC and 10 mM CC-930. Relative gene expressions were analyzed by RT-qPCR **(f)**, and protein level were analyzed by Western Blot **(g)**.

Data are represented as mean ± SD. *p ≤0.05; **p ≤0.01; ***p ≤0.001, Student's t test.

Fig 6: Mechanisms of AP-1-mediated anti-stress signaling in regulating TNBC SCC properties

(a) Schematic representation of predicted c-Jun/JunB heterodimer binding sites on CDKN1A and GADD45A promoter region.
(b,d) Overexpression of JunB leaded to up regulation of Cip/Kip and GADD45s. Relative gene expressions were analyzed by RT-qPCR **(b)**, and protein level were analyzed by Western Blot **(d)**. Data are represented as mean ± SD.
(c) Interfere with JunB would result in down regulation of AP-1 subunits, Cip/Kip and GADD45s. Relative gene expressions were analyzed by RT-qPCR.
(e) Overexpression of JunB result in robust tumorigenesis. MDA-MB-231 cells with overexpressing of JunB or control were injected into forth mammary fat pad in the right flank of nude mice. Overexpressing of JunB resulted in larger tumor formation, whether in tumor volume or tumor weight. Scale bar = 1 cm.
(e) Overexpression of JunB result in larger areas of tumor necrosis. Scale bars=2 mm; high-magnification scale bars=100 μm.
*p ≤0.05; **p ≤0.01; ***p ≤0.001, Student's t test.

Fig 7: CC-930 could reduce SCCs residual after chemotherapy in vivo

(a) Timeline of in vivo experiment. MDA-MB-231 cells were injected into forth mammary fat pad in the right flank of nude mice. After 1 week, 40 mice were randomly divided into 4 groups, treated with vehicle, TAC, CC-930 or combination. TAC was given by i.p. every week, and CC-930 was given orally every day. After 21 days of treatment, mice were sacrificed, and tumors were removed.
(b) Tumor volume and body weight were measured 3 times a week. CC-930 combined with TAC could effectively reduce the tumor volume and recurrence.
(c-d) Tumor weight and photographs.
(e) HE staining of tumor.

Fig 8: Schematic representation of AP-1 regulation in SCCs

c-Jun is at the center of AP-1 activity. N-terminal phosphorylation site of c-Jun contribute to AP-1 transcription activity, and C-terminal phosphorylation site of c-Jun prejudice to DNA binding affinity. Activation of JNK and ERK contribute to AP-1 transcription activity by phosphorylation of these two sites separately. c-Jun could form homodimer and form heterodimer dimer with c-Fos, promoting proliferation-related gene expression. JunB could from heterodimer dimer with c-Jun, inhibited proliferation-related gene expression through competitive binding, and promoting dormancy-related gene expression such as *CDKN1A* and *GADD45A*.

Supplementary Fig 1: Schematics of different label
BrdU/EdU can be incorporated into DNA during S phase instead of thymine.
Lipophilic dyes (PKH26 and Claret) label the phospholipid bilayer of cells through a hydrophobic tail.
Protein covalent binding dyes (CFSE and Violet) enter the cells by diffusion. The ester group got removed by intracellular esterase, and the fluorescent part of the dye covalently

bound to the available amino groups (including the side chain amino groups of lysine) of intracellular protein and intracellular portion of transmembrane protein.
eGFP and H2B fusion protein is expressed under the control of tetracycline responding element, thereby traces chromosomes and nucleus.
Alternative dyes with different fluorescence are listed on the right.

Supplementary Fig 2: Detailed data of each dyes' retained ratio on each day.

Supplementary Fig 3: Detailed data of each pair of dyes' retained correlations on each day.

Supplementary Fig 4: Detailed data of each pair of dyes' retained correlations on each day. R^2 was calculated with Person correlation.

Supplementary Fig 5: Detailed t_SNE plot of each dye on each day.

Supplementary Fig 6
(a) PI staining shoed SCCs enriched polyploid cells.
(b) Although $ALDH^+$ cells enriched more SCCs, the proportion of SCCs was still small.
(c) In vivo experiments suggested that SCCs have stronger metastatic capacity. SCCs and bulk cells were sorted as described above. 1000 cells were injected into tail vein of nude mice. Each n=6.
(d) SA-β-GAL staining showed SCCs we identified were not senescent cells. Scale bar = 50 mm.
(e) Representative image of the Transewell experiment. Scale bar = 40 mm.

Supplementary Fig 7: Detailed dyes' retained ratio of each treatment.

Supplementary Fig 8:
SCCs were enriched in chemokine signaling pathways and senescence-associated secretory phenotype (SASP)

Supplementary Fig 9
(a) High expression of FOS has no significant effect on the survival rate of overall breast cancer patients and ER^+ patients, and less effect on the survival of ER^- patients compared with TNBC patients. Data was acquired from TCGA-BRCA database.
(b) High expression of FOS has weak correlation with the survival rate of TNBC patients. Data was acquired from TCGA-BRCA database.
(c) TNBC patient with both *FOS*/*JUN* high expression had worse prognosis. Patients with both *FOS*/*JUN* gene expression > median gene expression were considered as high-expression group. Data was acquired from TCGA-BRCA database. n=84, total n=222.
(d) The effect of simultaneous high expression of AP-1 gene on the survival of TNBC patients. The data on the diagonal line is the effect of a single gene on patient survival.

Data was acquired from TCGA-BRCA database, total n=222.
(e) High expression of *FOS* or *FOSB*, or simultaneously high expression of *FOS* and *FOSB* is a poor prognostic factor for TNBC. Data was acquired from METABRIC database, and grouped according to the best cut-off.

Supplementary Fig 10
(a) SCCs were upregulated in AP-1 downstream genes, including *IL6*, *CXCl2*, *CXCL3* and *CXCL8*.
(b) SCCs were upregulated in RNA splicing genes.

Supplementary Fig 11: Detailed t_SNE plot of each treatment.

Supplementary Fig 12: Dual luciferase assay
All dual luciferase assays were performed in HEK293T cells.
(a) CC-930 could inhibit AP-1 transcription activity. Firefly luciferase was expressed via AP-1 response element (AP1RE), and Renilla luciferase was expressed via SV40 promoter. Relative luciferase activity was calculated using Firefly luciferase luminous intensity / Renilla luciferase luminous intensity (Luc / RLuc), and normalized with control group.
(b) JunB binds to CDKN1A and GADD45A promoter region and activate their expression. Firefly luciferase is expressed via CDKN1A/GADD45A promoter, Renilla luciferase is expressed via SV40 promoter. To determine promoter activity, relative Luciferase activity was calculated as described before, and normalized with each control group.
(c) Overexpression of JunB could upregulate AP-1 transcriptional activity. Firefly luciferase was expressed via AP-1 response element. Relative Luciferase activity was calculated as previously described, and normalized with control group.
Data are represented as mean ± SD. ***$p<0.001$. n.s. means no significant difference.

Supplementary Fig 13:
Body weight changes in mice in vivo. **(a)** Overexpression of JunB had no significant effect on body weight of mice. **(b)** TAC and combination treatment resulted in body weight loss.

Supplementary Fig 14:
Colony formation assay. $PKH26^+$ SCCs and $PKH26^-$ RCCs were sorted as described before. Cells were plated into 12-well plate with 500 cells/well. Cells were treated with 1 μm CC-930 or equivalent DMSO for 12 days. Cells were stained with crystal violet.

Supplementary Fig 15: full-size western blot images

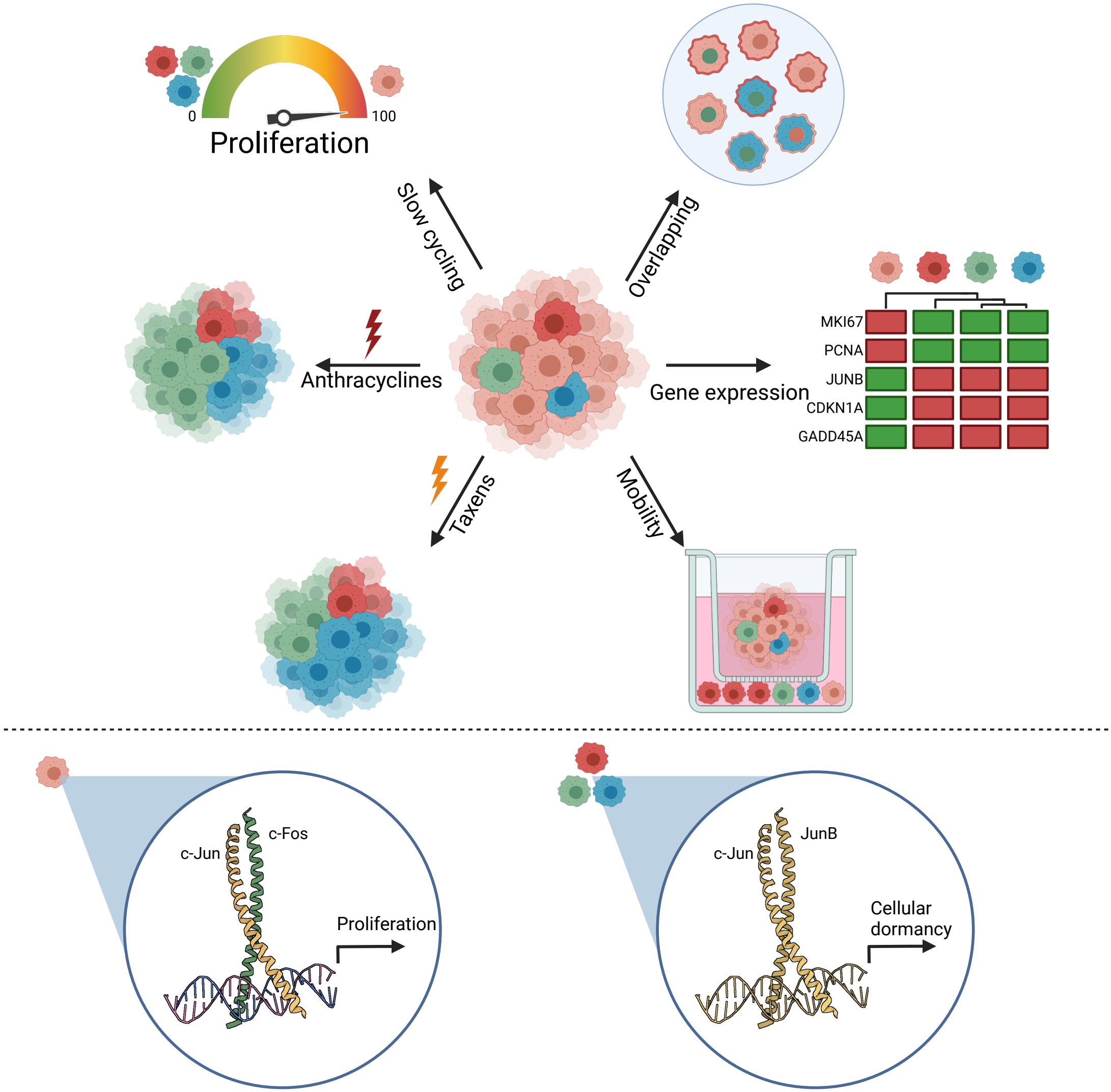
0
100
Proliferation
Slow cycling
Overlapping
Anthracyclines
Gene expression
MKI67
PCNA
JUNB
CDKN1A
GADD45A
Taxens
Mobility
c-Jun
c-Fos
Proliferation
c-Jun
JunB
Cellular
dormancy

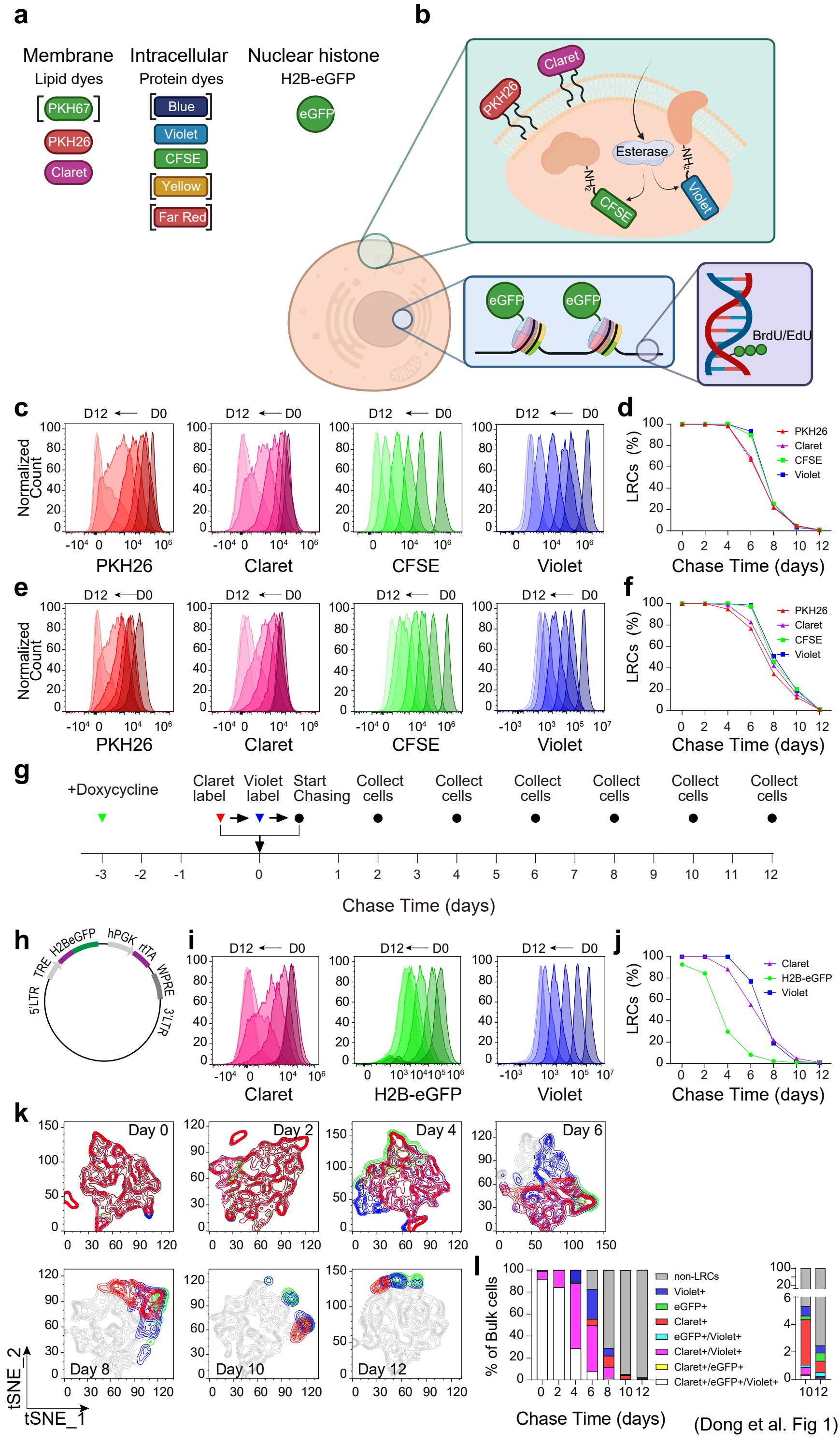

(Dong et al. Fig 1)

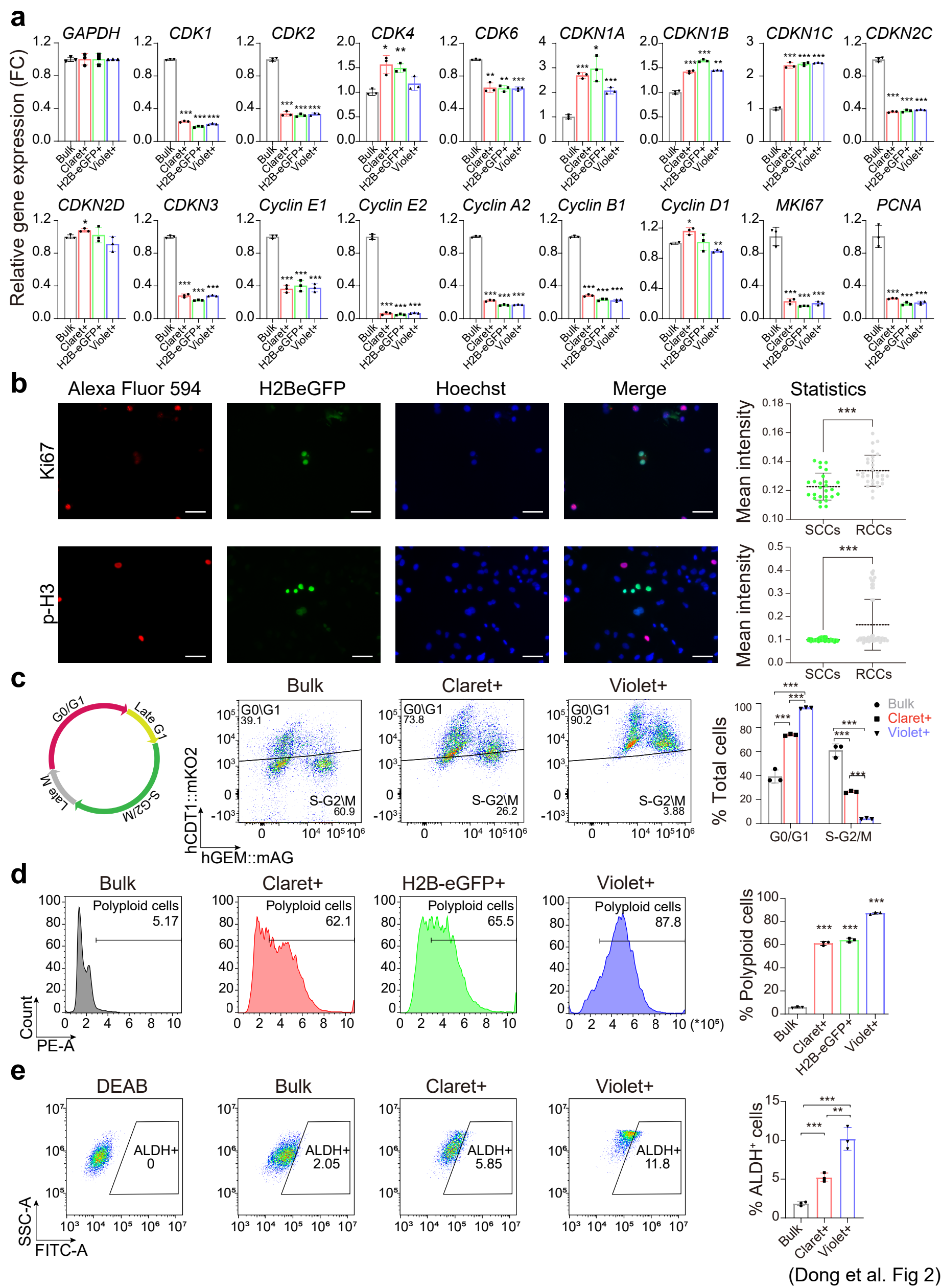

(Dong et al. Fig 2)

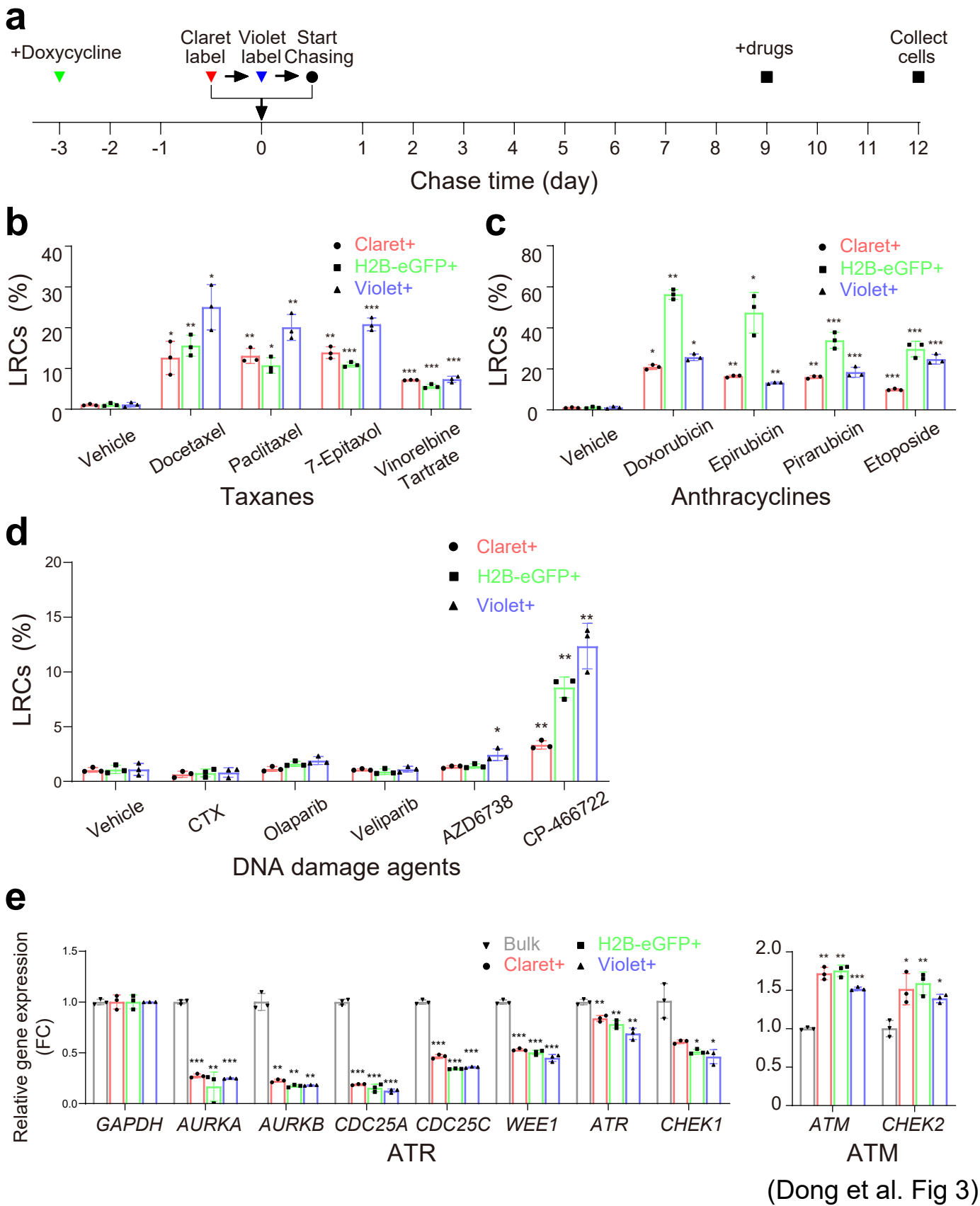

(Dong et al. Fig 3)

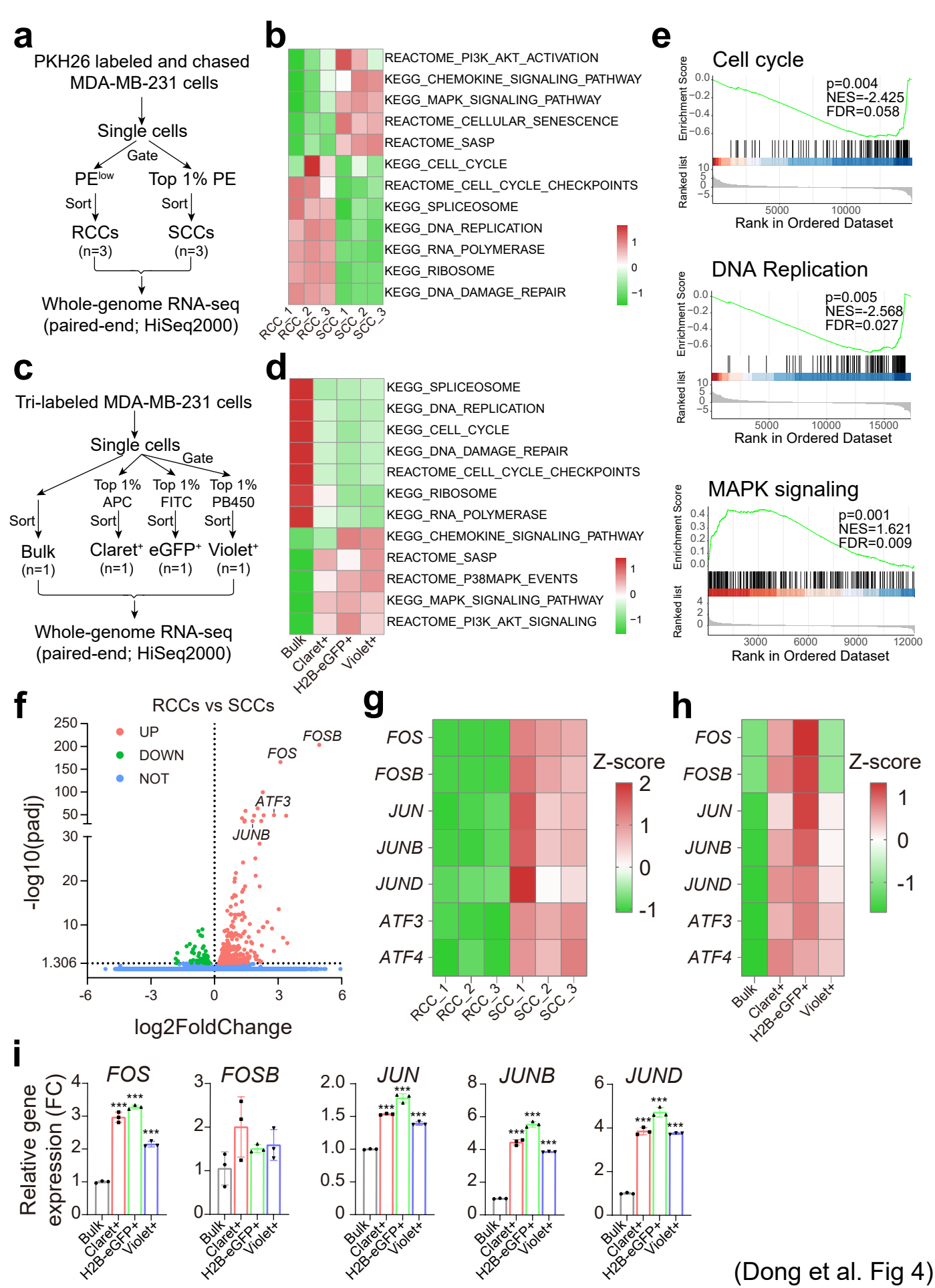

(Dong et al. Fig 4)

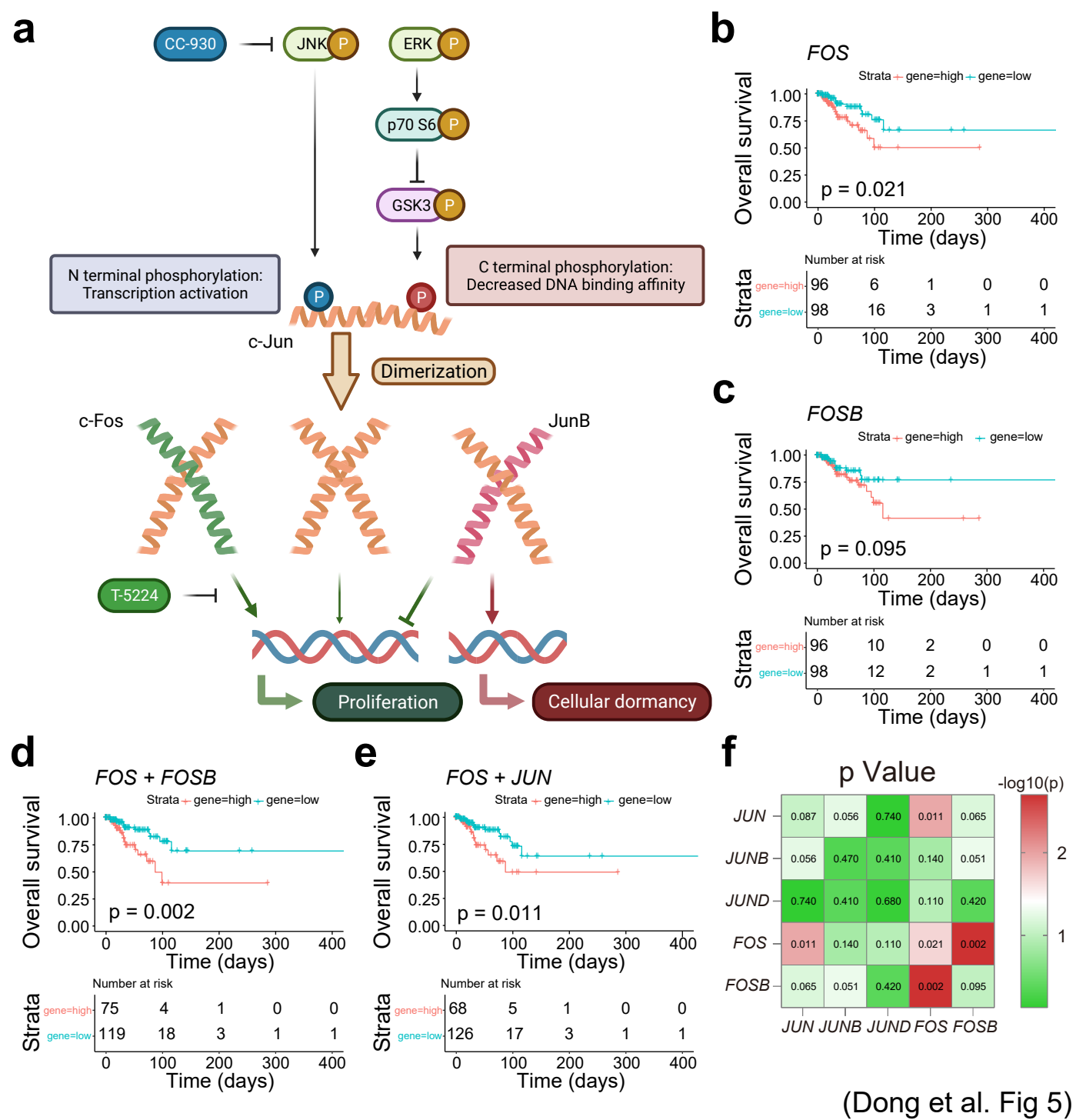

(Dong et al. Fig 5)

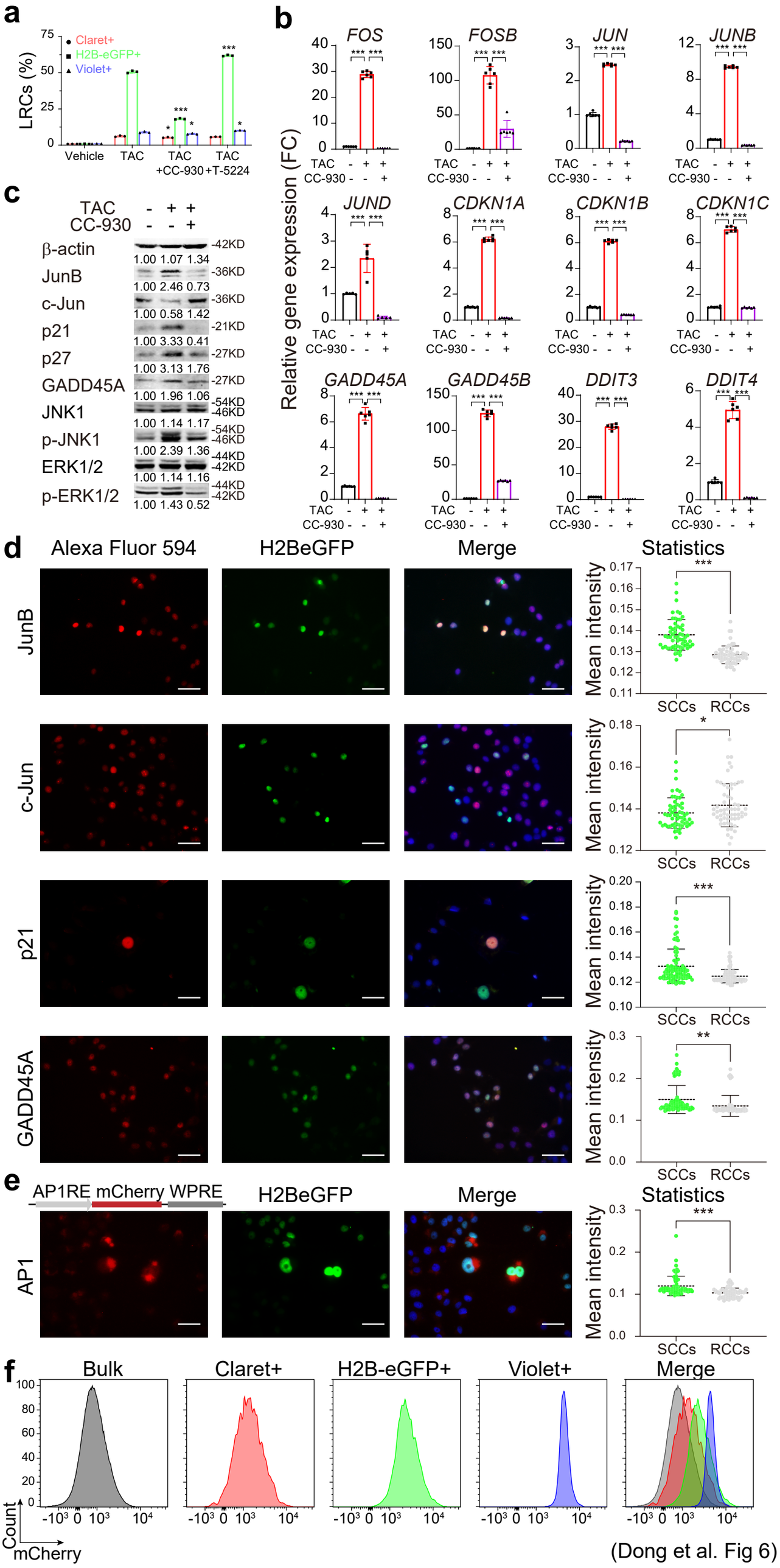

(Dong et al. Fig 6)

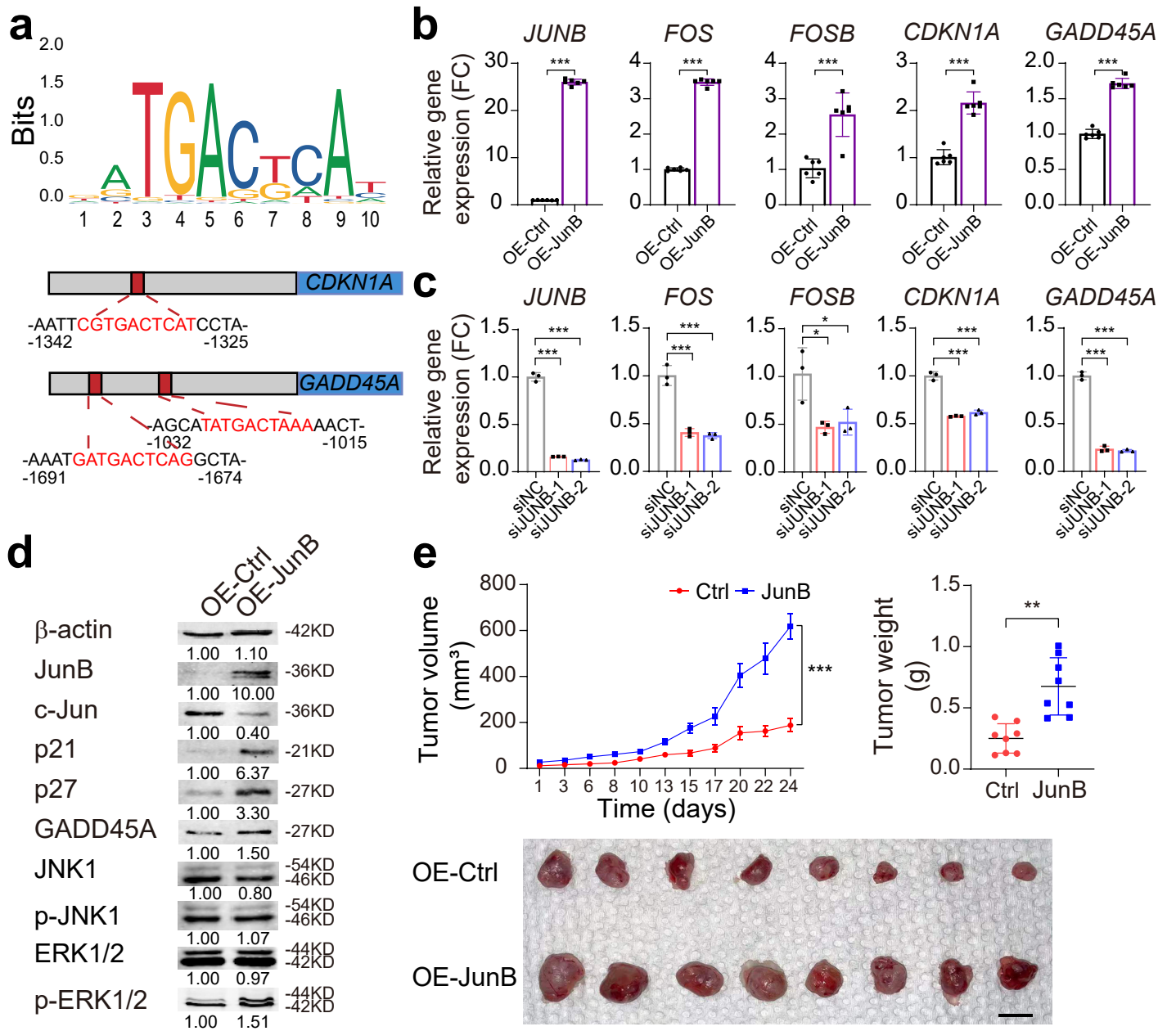

(Dong et al. Fig 7)

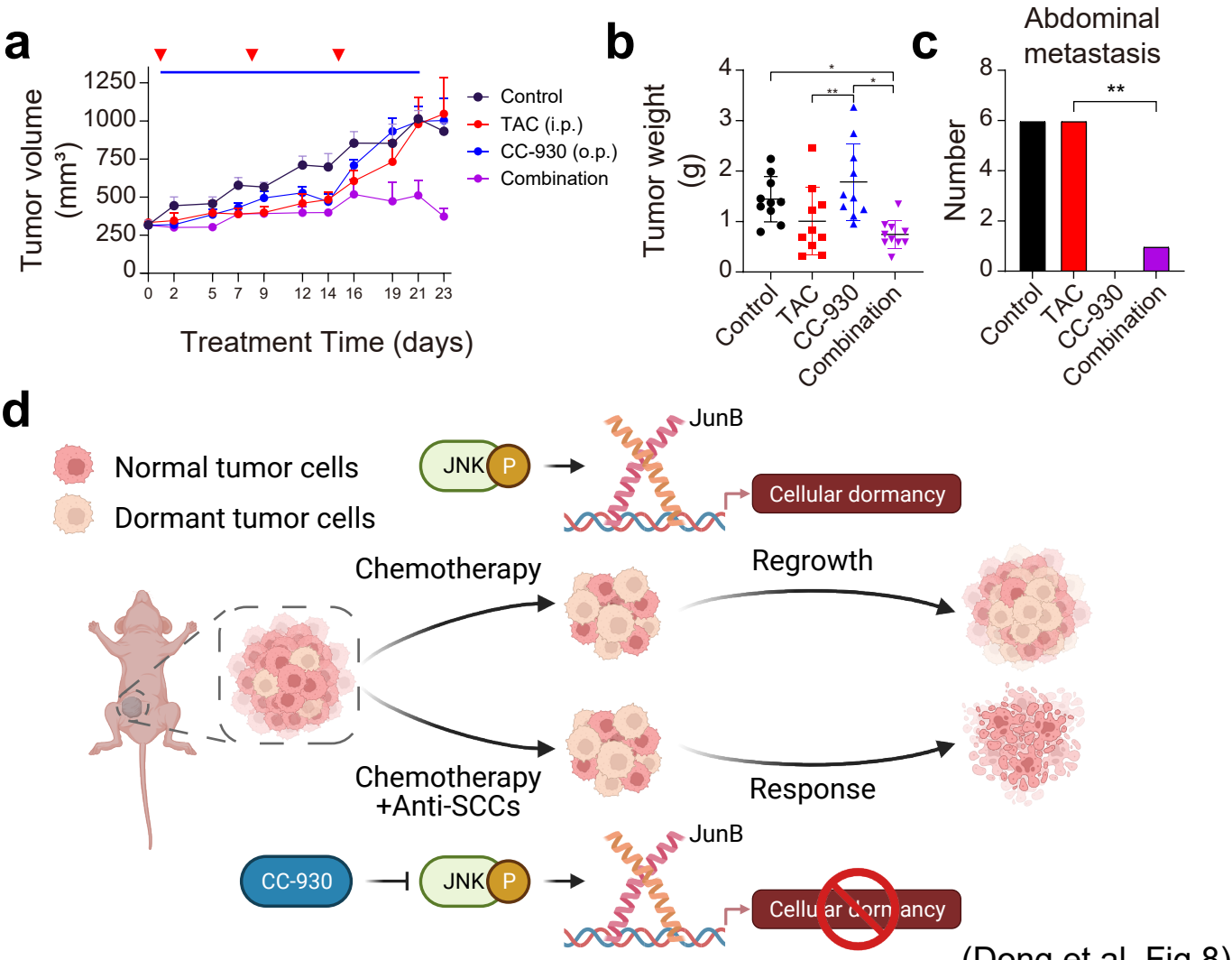

(Dong et al. Fig 8)